Journal of Solar Energy Research (JSER)

Journal homepage: jser.ut.ac.ir

Numerical study on the Performance enhancement of curved solar air heaters

Arman Taghavi[a], Abolfazl Hajizadeh Aghdam[b*]

[a,b]*Department of Mechanical Engineering, Arak University of Technology, Arak, Iran*

A B S T R A C T

In this study, the performance of a 3D curved solar air heater was simulated using fluent software. Then based on the available data an equation is presented to estimate the efficiency of heaters with different curves as well as the corresponding constraints. Increasing the curvature of the heater increases the thermal efficiency, but this is compounded by the cost of building the machine and the pressure drop. The higher the pressure drop the stronger the compressor will require to pump the air to the desired flow rate.

.

Keywords: Solar air heater; Curvature; Heat transfer; pressure drop

1. Introduction

Nowadays, the need to supply the energy needed in different parts of the industry is felt by using solar energy and increasing its production. The efficiency of the devices used in this area is a key parameter that determines whether solar energy is efficient in the sector or not.

The efficiency determined for these types of devices is defined by the amount of energy received by the carrier system as well as the amount of energy loss.

The higher the energy supply to the converter and the lower the heat loss, the efficiency is greater. [1]

Among heaters used in the solar industries, air-heaters are suitable for low and medium temperatures. [2]

Its applications include air conditioning and drying processes. [3], [4], [5]

An important problem with this is that the thermal properties of the air are lower than other fluids.

This is why most of the limitations in the design of these heaters are due to the need for specific designs and special raw materials that incur high manufacturing costs on both sides. [6]

Since the conductivity of the absorbent plates and the corrosion resistance have little effect on the performance of solar air heaters, the improvement of the material properties have used is limited to the optical properties, surface texture, electrolytic and chemical methods. [7]

However, the performance of these heaters is very sensitive to other complex phenomena observed through the heat transfer in the flow channel.

Studies show that the roughening of the inner surface of the heater improves the performance of the heater due to an increase in the turbulence of flow followed by an increase in Nusselt number which increases the forced

convection heat transfer between the air and the adsorbent surface.

Of course, pressure drops occur along with this. The best type of roughness heater interior is the V-shaped.

The results show that the narrower flow channel, increases the spectral absorption component of the glass coating on the adsorbent surface, as well as decreasing its emissivity, determining the inlet flow rate at amounts greater than 0.1 kg / s, and keeping the inlet temperature close to the set at about Ambient temperature are some of the factors that improve performance. [7], [8]

The optimum curve for the heater is determined in the actual model is 3 m and the inlet flow rates are 0.0472, 0.029 and 0.0172 kg / s.

The result of the experimental study shows that increasing the curvature, in addition to increasing the surface area of the adsorbent relative to the occupied area, increases the centrifugal force to the fluid and reduces the amount of pressure drop, especially when artificial roughness on surfaces are created.

In terms of the type of material used for making this type of heater, the same materials can be used in common flat heaters, so there will be no additional weight or cost of manufacture.

Energy and exergy analysis shows that increasing the mid-level porosity increases the heater efficiency by 30% and also by the second law increases the pressure drop. Therefore, the cost of manufacturing the device as well as the power required in the air pump system is increased and economically limited. [10]

In air-heaters that use phase-shifting materials to store energy, the geometry of the two substrates with circular capsules increases storage capacity. [12] In a typical air-heater, paraffin is used as a phase-shifting material and air as a heat-absorbing fluid. The findings show that the mean thermal efficiency in summer is significantly higher than in other seasons. [13] Paraffin is inexpensive and easy to access; it is easy to use and has good chemical stability. [14] In an air-heater with a mechanism based on free convection heat transfer, the use of cherry kernel as a Sensible heat storage source increases the thermal efficiency. [15] Baffle placement on the heater surface increases energy and exergy efficiency. [16]

Under windy condition the heat loss from SAH (Solar air-heater) to surrounding is lower for curved SAH at θ=0°, 60° in windward, 30° in leeward and 30° in tranquil-condition in comparison to flat SAH. [17]

half-trapezoidal and quarter-circular shape ribs on the absorber surface, shows maximum increase in thermal performance i.e. 17% and 16%, respectively, however frictional loss for quarter-circular ribs is less by about 10% when compared to trapezoidal shape ribs. [18]

2. Computational Model Description

The actual model span is 1.6 m long, 40 mm thick and 80 cm deep, and its longitudinal curve is part of the circle, resulting in a heater span of 1.28 m^2 (A_c = 1.28 m^2). The central angle of the arc is about 30.5 degrees. The inlet temperature of the heater is approximately equal to the ambient temperature ($T_i \approx T_a$) and the floor surface and the side walls are insulated. Figures 1 [9] and 2 [6] show the body of the model in question.

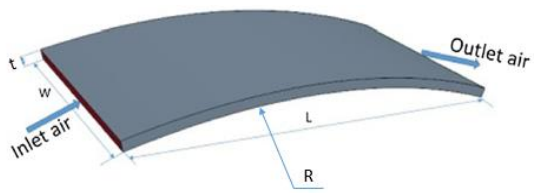

Figure 1. A schematic of the heater

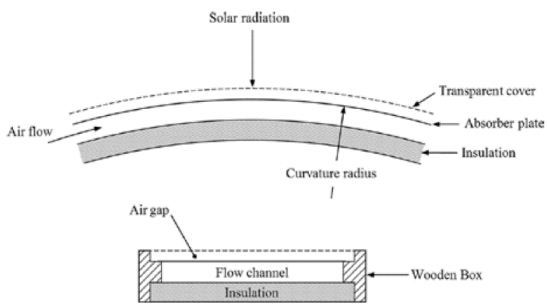

Figure 2. Heater details

The dimensions of the simulated model for "validation", as shown in figure 1, are exactly similar to the actual model; also, the arc span of the floor of the heater is 1.6 m in length, not the absorption surface arc. Subsequent simulations assume a constant length of 1.6 correspondings to the aperture surface. This makes the heater edge not to exceed from the considered area on the ground as the curvature of the heater increases, and the analysis results are completely focused on the adsorbent surface. Simulation is performed for 9 different "central" angles of the arc (from 10 to 90 degrees).

3. Boundary Conditions

Simulation and validation are performed for three mass fluxes of 0.5375, 0.90625 and 1.475 kg / s.m^2 (equivalent to 0.0472, 0.029 and 0.0172 kg / s) and various heat fluxes (based on experimental study [6]). In the experimental data, the unit of heat flux analyzed is watts per unit area of the heater span. Curving the heater increases the absorption surface. It is like having an increase in flat plate heater length. Because the heater curvature (center angle is approximately 30.5 degrees) is low and the heater is approximate to the flat case, the constant heat flux boundary condition for the absorber wall can be used instead of the radiation. The following boundary conditions are used to validate empirical data:

$$I = 800\,\frac{W}{m^2}\,, T_{in} = 298.15\,K\,, \dot{m} = 0.0472\,\frac{kg}{s}$$

The incoming flux is in watts per unit area of the "heater span". In the present study, only the mass flow rate of 1.475 kg / s.m^2 (mass flow rate of 0.0472 kg / s) is considered. The heat flux is generated using the sun's radiation perpendicular to the heater span (in line with the normal vector of the span of the plate); Therefore, in this case, the direction of heat flux applied at each point of the arc is not perpendicular to the arc. The direct heat flux size is 900 watts per unit area of the heater span and the diffuse solar irradiation is 200 watts per unit area of the heater span. The spectral transmission component of the glass is 0.8 and the spectral transmission component is 0.1.

4. Mesh Analysis

Fluent software is used for analysis. Before proceeding to the results, the mesh independence analysis must be done for the desired geometry so that the results do not change as the mesh becomes finer. For this purpose, the average output temperature of the heater is set. The mesh independence analysis and mesh shape are shown in figures 3 and 4, respectively. Because each heater with its central angle requires a separate mesh independence analysis, the volume of computation will increase; so a study is performed for the heater with a 10 degrees angle and is Generalized to the other angles. The method is examined at each step of the analysis is considering the maximum element size, rather than the number of nodes. In the present analysis, calculations were made for maximum sizes of 2.5, 3, 3.5, 4, 5, 6, 7 and 8 mm. Finally, according to figure 3, all calculations are done with a maximum size of 3 mm (2 million nodes for a 10 degrees arc).

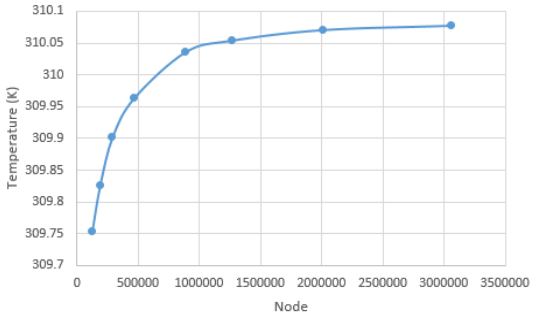

Figure 3. mesh analysis diagram; the average output temperature of the heater versus the number of mesh nodes (Central angle of the arc: 10 degrees)

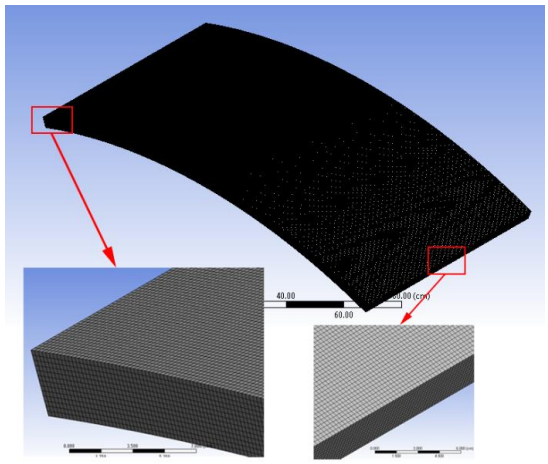

Figure 4. Heater mesh with 10 degrees central arc angle

5. System Analysis

The following equations are used to calculate the heater practical thermal efficiency and the error percentage:

$$\eta_{th} = \frac{\dot{m}\,C_p\,\,(T_{out} - T_{in})_{exp}}{I.A_c} \qquad (1)$$

$$Error = \frac{\dot{m}\,C_p\,\,(T_{out} - T_{in})_{num} - I.A_{abs}}{I.A_{abs}} \times 100 \qquad (2)$$

A_c and A_{abs} are the aperture surface area and heater absorbent surface area, respectively. Based on these correlations, the relationship between the flow rate and the temperature parameter ((ΔT_{exp} / I), the flow rate and the

efficiency variations, as well as the difference between the software responses and the exact answer can be measured. Theoretical thermal efficiency is also obtained from the following relation: [6]

$$\eta_{th} = F_0(\tau\alpha) - F_0 U_L \frac{T_{out} - T_a}{I} \quad (3)$$

F_0 is the heat removal coefficient based on the output air temperature, τα the result of multiplying the spectral absorption and transmission component and U_L Overall heat dissipation coefficient in W / m^2.K. As the flow rate increases, the pressure drop in the air pump system increases, reducing the effective efficiency of the system. Effective efficiency is:

$$\eta_{eff} = \frac{\dot{m}\, C_p\ (T_{out} - T_{in})_{exp} - \frac{P_{mec}}{C_f}}{I.A_c} \quad (4)$$

$$P_{mec} = \frac{\dot{m}\Delta p}{\rho} \quad (5)$$

P_{mech} is the mechanical power and the conversion factor, C_f, is considered to be 0.18.

The main cause of the increase in efficiency in this study is the increase in heater curvature and consequently, the increase in adsorption surface and the thermal efficiency is defined accordingly. According to the law of energy conservation:

$$\eta_{th} I.A_{abs} = \dot{m}\, C_p \Delta T_a \quad (6)$$

ΔT_a is The theoretical (analytical) temperature difference.

$$\frac{\dot{m}\, C_p\ (T_{out} - T_{in})_{exp}}{I.A_c} I.A_{abs} = \dot{m}\, C_p \Delta T_a \quad (7)$$

$$\Delta T_{exp} \frac{A_{abs}}{A_c} = \Delta T_a \quad (8)$$

As can be seen in this equation ΔT_{exp} and ΔT_a are equal when the area of absorption and span are equal.

As can be seen in this respect ΔT_{exp} and ΔT_a are equal when the area of absorption and span is equal. Therefore, the above equation is incomplete due to its definition of efficiency and is modified as follows:

$$\eta_{th} \frac{A_c}{A_{abs}} I.A_{abs} = \dot{m}\, C_p \Delta T_a \quad (9)$$

The other result is that since the efficiency is considered to be 1 in the software, the latter relation is used to compare the data obtained from the present simulation and experimental study. Thus the error percentage can also be calculated from the following relation:

$$Error = \frac{\eta_{th} \frac{A_c}{A_{abs}} \Delta T_{num} - \Delta T_{exp}}{\Delta T_{exp}} \times 100 \quad (10)$$

The area of the adsorbent surface is calculated as follows:

$$\sin\frac{\theta}{2} = \frac{L}{2R} \quad (11)$$

$$R = \frac{L}{2\sin\frac{\theta}{2}}, \theta = 2\,\text{asin}\frac{L}{2R} \quad (12)$$

Where L is the length of the heater span, R the radius of curvature of the absorption surface and θ the corresponding arc angle in radians (Figure 1).

So d (absorption surface span) is:

$$d = R.\theta \quad (13)$$

Thus:

$$A_{abs} = w\frac{L}{2\sin\frac{\theta}{2}}\theta = 2\,w\,R\,\text{asin}\frac{L}{2R} \quad (14)$$

6. Governing Equations

Continuity equation:

$$\frac{\partial \rho}{\partial t} + \nabla.(\rho V) = 0 \quad (15)$$

Momentum equations include k-ε equations:

$$\frac{\partial(\varepsilon\rho)}{\partial t}+\nabla.(\rho\varepsilon V)=\nabla.\left(\frac{\mu_t}{\sigma_\varepsilon}\nabla\varepsilon\right)+C_{1\varepsilon}\frac{\varepsilon}{k}2\mu_t E_{ij}.E_{ij}-C_{2\varepsilon}\rho\frac{\varepsilon^2}{k} \quad (16)$$

$$\frac{\partial(\rho k)}{\partial t}+\nabla.(\rho kV)=\nabla.\left(\frac{\mu_t}{\sigma_k}\nabla k\right)+2\mu_t E_{ij}.E_{ij}-\rho\varepsilon \quad (17)$$

V The velocity component in the desired direction, E_{ij} the strain rate tensor, μ_t represents the eddy viscosity, σ_k ، σ_ε ،$C_{1\varepsilon}$ ،$C_{2\varepsilon}$ are the adjustable coefficients.

Energy equation:

$$\rho C_p\left(\frac{dT}{dt}+\nabla(TV)\right)=\nabla^2(kT) \quad (18)$$

In this relation, k represents the conductivity.

Reynolds number:

$$Re=\frac{Inertia\ force}{Viscous\ force}=\frac{\rho\,V\,D_h}{\mu} \quad (19)$$

P1 radiation model governing equation:

$$\nabla.(\Gamma_{rad}\nabla R_I)+\alpha(4\sigma T^4-R_I)=0 \quad (20)$$

σ Stephen Boltzmann constant, a the spectral absorption component, R_I incident radiation, Γ_{rad} is defined as:

$$\Gamma_{rad}=\left(3(a+s)-C_g s\right)^{-1} \quad (21)$$

s represents the dispersion coefficient in m^{-1} and C_g represents the symmetry coefficient for the dispersion function of the material phase.

7. Global Solar Radiation

The heater surface is considered to be a countless element of the surface area dA with each other and the angle of each horizon equal to β_i; Therefore:

$$I_{\beta_i}=I_{hB}(\cos\beta_i+\tan\theta_z\sin\beta_i\cos(\gamma_s-\gamma))+I_{hD}\frac{1+\cos\beta_i}{2}+I_h\,\rho_g\frac{1-\cos\beta_i}{2} \quad (22)$$

I_{hB} Direct beam solar radiation on a horizontal surface, (W/m^2)

I_{hD} Sky diffuse solar radiation on a horizontal surface, (W/m^2)

I_h Global solar radiation on a horizontal surface, (W/m^2)

θ_z Solar zenith angle, (°)

γ Surface azimuth angle, (°)

γ_s Solar azimuth angle, (°)

ρ_g Ground reflectance

It is integrated From the above relation around the heater absorption area, as can be seen below so that

$\beta-\varphi\le\beta_i\le\beta+\varphi$:

$$\varphi=\frac{L}{2R} \quad (23)$$

And β is the angle of deviation of the heater in the middle of the surface.

$$I_\beta=I_{hB}(\cos\beta+\tan\theta_z\sin\beta\cos(\gamma_s-\gamma))+I_{hD}\frac{1+r\cos\beta}{2}+I_h\,\rho_g\frac{1-r\cos\beta}{2} \quad (24)$$

$$r=\frac{\sin\varphi}{\varphi} \quad (25)$$

In the validation model, the value of φ is relatively small (approximately 0.267 radians), so the value of r equals one and eq. (24) becomes identical to that of incident solar radiation on a plane surface tilted with an inclination angle β. [6]

Therefore, the constant-flux simulation does not differ much from the radiation and specific solar radiation directions with the curved heater surface elements.

8. Results & Discussions

In the case of the curved heater, the k-ε model provides the closest answers to the experimental data. [9]

The error percentage for low mass flux is 5.16, medium flux is 5.6 and high flux is 6.1%. The central arc angle is 30.5 degrees and the experiments are conducted from 10 am to 3 pm with a half-hour interval.

Table 1 regarding to mass fluxes of 0.5375, 0.90625 and 1.475 kg / s.m^2, respectively. In the set of figures A5, B5 and C5, as can be seen, from 10 o'clock the sun rises at about noon and decreases from hour to hour. As the ambient temperature flux increases, the heater performance increases. the output temperature also increases so that the difference between the inlet and outlet temperatures increases. Increasing the flow rate increases the turbulence of flow and the Nusselt number. This means that at higher flow rates the heat transfer between the heater surface and the indoor air is increased and the heat absorption is increased which means an increase in the efficiency.

When the flow rate is low, the fluid has more opportunity to absorb heat, so the outlet temperature is higher at lower flow rates. But due to less turbulence the heat received is lower than the dissipation, so the efficiency is lower.

Table 1. Comparison of numerical and experimental data for three different mass fluxes

		Heater air temperature differences (°C)		
Mass flux (kg/s.m^2)	Incident heat flux (W/m^2)	Experimental study result [6]	Present simulation result	Error percentage (%)
1.475	820.5	13	13.79441	6.110816
0.90625	800	16.5	17.42504	5.606282
0.5375	810.3	17.5	18.40288	5.157398

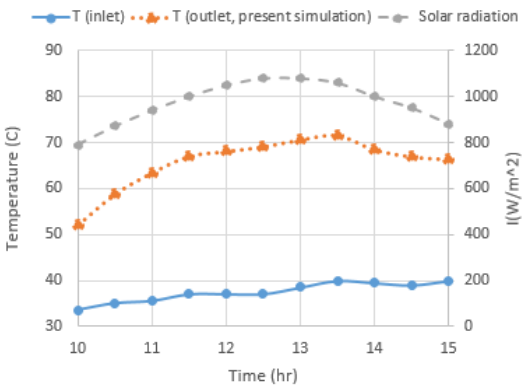

Figure A5. Comparison and analysis diagram of numerical and experimental data for the mass flux of 0.5375 kg/s.m^2

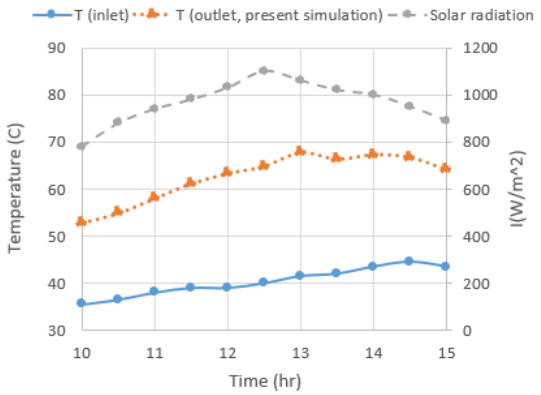

Figure B5. Comparison and analysis diagram of numerical and experimental data for the mass flux of 0.90625 kg/s.m^2

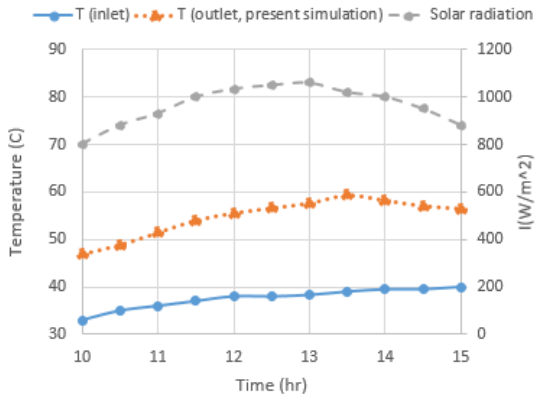

Figure C5. Comparison and analysis diagram of numerical and experimental data for the mass flux of 1.475 kg/s.m^2

Figure A6 shows the efficiency versus the temperature parameter. The results show that the efficiency increases with an increasing flow rate.

If these data come together and fitted to a line, the resulting line equation is:

$$\eta = -19.54\frac{\Delta T}{I} + 0.9 \quad (26)$$

If the heater is a flat plate, the equation for this line is as follows: [11]

$$\eta = -8\frac{\Delta T}{I} + 0.56 \quad (27)$$

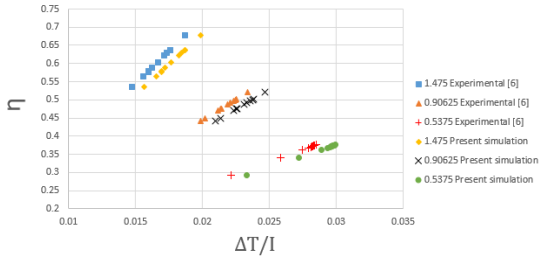

Figure A6. Efficiency versus temperature diagram; Comparison and analysis of numerical and experimental data (The side numbers are the mass fluxes in kg/s.m^2)

The two lines are intersecting at a point (Figure B6) On the other hand, according to figures A6 and B6, the effect of heater curvature on increasing thermal efficiency decreases with decreasing flow rate; Therefore, if the flow rate is too low, the curvature generally loses its effect on thermal efficiency. In turn, the effect of curvature increases with increasing flow rate and the efficiency increases more; because curved and flat heater lines diverge due to the increasing flow rate (To the left).

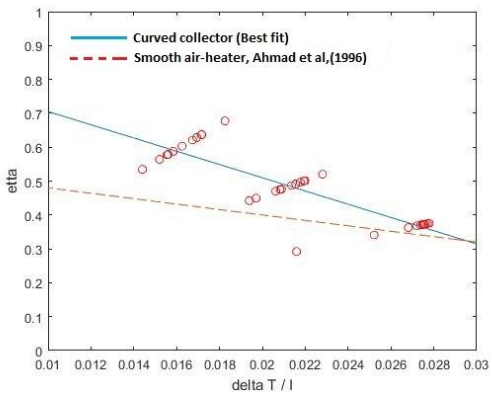

Figure B6. Comparison between curved and flat heater in efficiency versus temperature diagram

Figures A7, B7, and C7 show temperature difference variations versus heat flux for low, medium and high mass flow rates, respectively.

According to the results, as the applied heat flux increases, the temperature difference between inlet and outlet increases. Although increasing the amount of radiation increases the ambient temperature, the heater performance due to its efficiency is such that it increases the temperature difference. But sometimes because of low efficiency, improper heater geometry or other factors, the temperature difference stays or decreases as the heat flux increases.

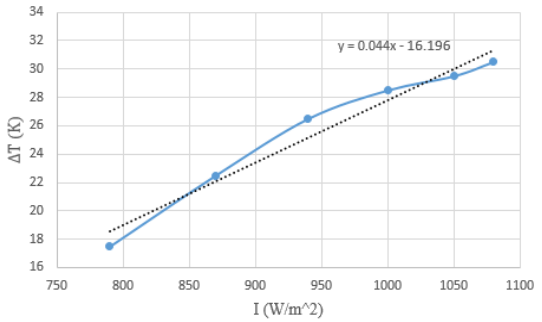

Figure A7. Temperature difference versus heat flux with a linear fit for the mass flux of 0.5375 kg/s.m^2

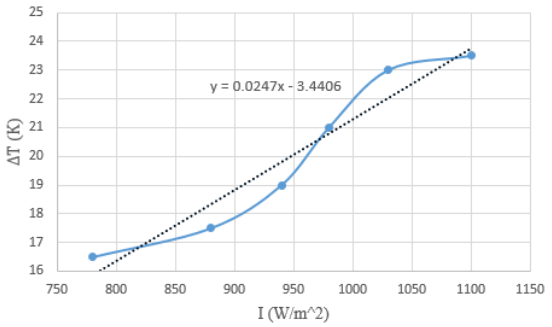

Figure B7. Temperature difference versus heat flux with a linear fit for the mass flux of 0.90625 kg/s.m^2

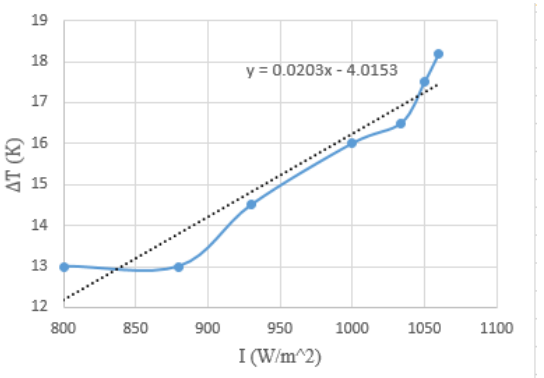

Figure C7. Temperature difference versus heat flux with a linear fit for the mass flux of 1.475 kg/s.m^2

$$\Delta T = aI + b \tag{28}$$

Where a is the slope of the lines in the above diagrams and b is the width of their origin; On the other hand:

$$\eta_{th} = \frac{\dot{m}\, C_p\ (T_{out} - T_{in})_{exp}}{I.A_c} = \frac{\dot{m}\, C_p (aI + b)}{I.A_c} \tag{29}$$

Given that at constant heat flux due to solar radiation, increasing curvature and increasing heat flux give the same result, then the two can be equated.

$$I_{cte}A_{var} = I_{var}A_{cte} \quad (30)$$

$$I_{var} = \frac{I_{cte}A_{var}}{A_{cte}} \quad (31)$$

cte index means constant, var index means variable, I_{var} equivalent to I in later relations, and A_{var} previously computed in the system analysis section, as A_{abs}, so according to the "validation" model:

$$A_{cte} = 0.8\left(\frac{1.6}{2\sin\left(\frac{30.5}{2}\,deg\right)} + 0.04\right)(30.5\,deg)\frac{\pi}{180}$$
$$= 1.312\,m^2, R = 3.082\,m$$

$$I = \frac{2\,w\;I_{cte}\,R\,\mathrm{asin}\frac{L}{2R}}{A_{cte}} \quad (32)$$

Consequently:

$$I = 1.524\,w\,I_{cte}\,R\,\mathrm{asin}\frac{L}{2R} \quad (33)$$

By placing the above relation in the efficiency formula as well as dimming the radius of curvature as R /L:

$$\eta_{th} = \frac{\dot{m}\,C_p(a(1.524\,w\,L\,I_{cte}\frac{R}{L}\mathrm{asin}\frac{1}{\frac{2R}{L}}) + b)}{(1.524\,w\,L\,I_{cte}\frac{R}{L}\mathrm{asin}\frac{1}{\frac{2R}{L}}).A_c} \quad (34)$$

If the desired heat flux value and the radius of curvature of the heater are to be estimated according to the mass flow rate, it is sufficient to calculate the a and b values from the set of figures A7, B7 and C7 for the three corresponding flow rates and linearly fitted. To graph the efficiency in terms of flow rate. From here we can estimate the heater efficiency in different flow rates. The same can be done for heat flux by considering the flow rate constant and determining the efficiency at different heat fluxes. It should be kept in mind, however, that based on the analysis of the radiation flux, as was done in the preceding sections, it should be possible to consider the effect of the sun's radiation at approximately constant-heat flux case.

In general, since ΔT is a function of I and I is also a function of the radius of curvature of the heater, we can write:

$$\eta_{th} = \frac{\dot{m}\,C_p\,f(\frac{R}{L})}{\left(1.524\,w\,L\,I_{cte}\frac{R}{L}\mathrm{asin}\frac{1}{\frac{2R}{L}}\right).A_c} \quad (35)$$

Accordingly, more precise results can be reached by obtaining a more precise relationship between the temperature difference and the heat flux. In different parts of the world, if a curved heater is to be used, a heater with certain parameters is first constructed and tested, and the performance of other types of curved heaters is estimated based on the recent relation.

In the following, a numerical investigation of the effect of the central arc angle of the heater on several important parameters is discussed. These parameters include the overall rate of heat transfer, pressure drop, temperature differences and finally a dimensionless parameter called TEF that incorporates the above parameters.

TEF is the coefficient of performance of the heater, which is the rate of heat transfer relative to the coefficient of friction:

$$f = \frac{D_h}{L}\frac{\Delta p}{\frac{1}{2}\rho V^2} \quad (36)$$

$$TEF = \frac{Q}{Q_0}\left(\frac{f}{f0}\right)^{-\frac{1}{3}} \quad (37)$$

In flat heaters, L is considered to be the heater length, but in the curved heater, the increase in length is not a positive effect on performance because the increase in length is due to the increase in arc length and practically causes an increase in cost.

Figures 8, 9 and 10 show the above parameters as well as the thermal efficiency of the heater in terms of the central angle of the heater.

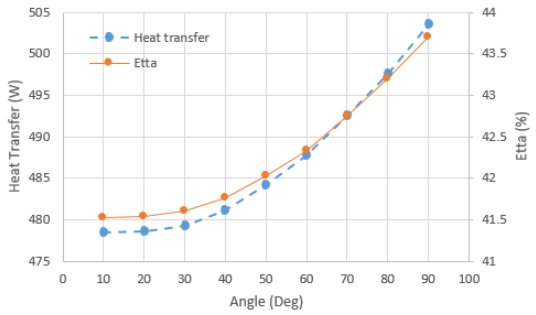

Figure 8. Diagram of thermal efficiency and overall heat transferred versus central arc angle of the heater

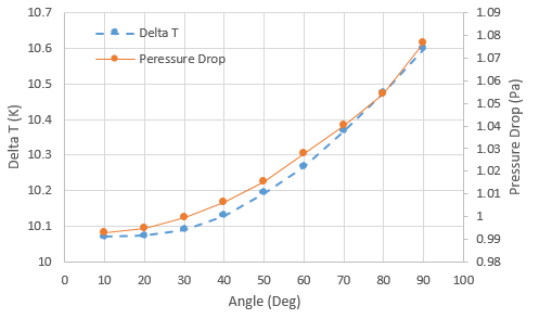

Figure 9. Diagram of pressure drop and overall temperature difference versus central arc angle of the heater

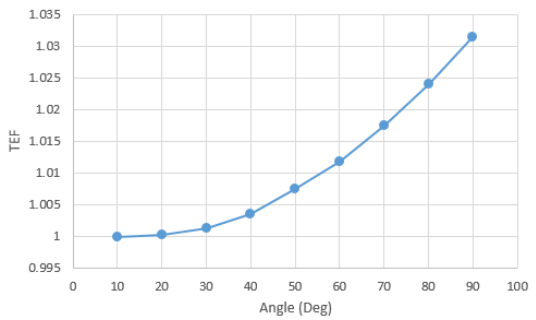

Figure 10. Diagram of TEF versus central arc angle of the heater

As the central arc angle increases, the radius of curvature decreases, so recent figures show that the "slope" of the graphs is inversely related to the radius of curvature. This indicates that in a relationship in which the thermal efficiency is expressed in terms of the radius of curvature, the temperature function in terms of the radius of curvature will have a downward concavity (or more generally, a negative slope).

$$\int \vec{I}_{cte} \cdot d\vec{A}_{var} = I_{cte} A_{var} \tag{38}$$

The right-hand side of the equation is similar to the previous one except that for the convenience, A_{cte} is considered the area corresponding to the flat heater. The angle between the vector I_{cte} and dA_{var} is always 90 to 180 degrees. So the cosine of the angle between them is negative; On the other hand, the direction of the vector I_{cte} is downward and is defined as follows:

$$\vec{I}_{cte} = -I_{cte}\hat{k} \tag{39}$$

So the left-hand side of the equation is simplified as follows:

$$\int_{-\frac{\theta}{2}}^{\frac{\theta}{2}} I_{cte}\, dA \cos\left(\frac{\theta}{2}\right) = I_{cte} \int_{-\frac{\theta}{2}}^{\frac{\theta}{2}} R.w \cos\left(\frac{\theta_1}{2}\right) d\theta_1 = 2R.w.I_{cte} \left(\sin\left(\frac{\theta_1}{2}\right)\right)_{-\frac{\theta}{2}}^{\frac{\theta}{2}} \tag{40}$$

Here we have:

$$4R.w.I_{cte} \sin\left(\frac{\theta}{4}\right) = I_{var}\,(L.w) \tag{41}$$

$$I = I_{var} = 4\frac{R}{L} I_{cte} \sin\left(\frac{\theta}{4}\right) \tag{42}$$

$$\eta_{th} = \frac{\dot{m}\, C_p\, (T_{out} - T_{in})_{exp}}{I.A_c} = \frac{\dot{m}\, C_p\, f\left(\frac{R}{L}\right)}{4\frac{R}{L} I_{cte} \sin\left(\frac{\theta}{4}\right)(L.w)} \tag{43}$$

$$\eta_{th} = \frac{\dot{m}\, C_p\, f\left(\frac{R}{L}\right)}{4R.w.I_{cte} \sin\left(\frac{\theta}{4}\right)} \tag{44}$$

Here R is the radius of curvature of the arc corresponding to the absorbent surface.

The limitation of this method is that it is assumed to direct the sun's radiation along the normal vector of the aperture plane.

Figures 11 and 12 show several important simulation contours. Contours belong to the model with a central angle of 40 degrees.

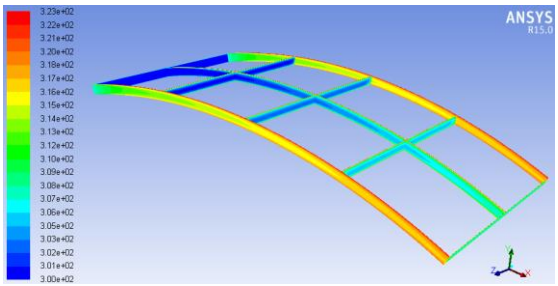

Figure 11. Static temperature contour in Kelvins, the heater with 40 degrees central angle (The left side is the flow inlet.)

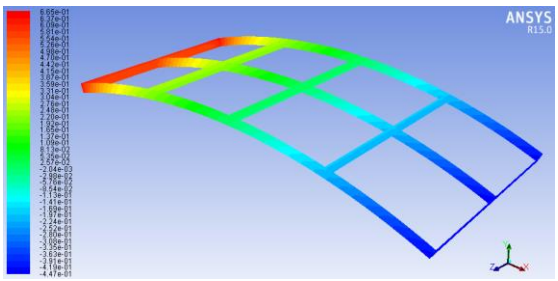

Figure 12. Static pressure contour in Paskals, the heater with 40 degrees central angle (The left side is the flow inlet.)

9. Conclusions

The use of the curved heater increases the thermal efficiency due to the occupied surface. Increasing the flow rate not only increases the efficiency but also increases the "rate" of the efficiency increase. This means that with the increase in flow rate the effect of the heater curvature is greater and with the flow rate decreasing from time to time the curved heater will be almost no different from the flat heater which is not economically feasible. According to the extracted relation, it is possible to estimate the heater efficiency in different flow rates by considering a certain amount of heat flux (eg heater analysis at a particular hour of the day), or vice versa, for a given flow rate, What effect do the different heat fluxes have on efficiency of the heater. In the final equation presented for calculating the efficiency, the sun's radiance is assumed to be along the normal vector of the aperture plane, but this relation is general and does not a necessity to the central arc angle be small. (The curved heater is estimable by the flat plate case.) At larger angles, the difference between the effect of the sun's radiation and the constant heat flux boundary condition is sharp, but the first relation is simpler and more functional if the conditions are present, not needed to the solar radiation be perfectly perpendicular to the aperture. If the curved heater is to be used in different parts of the world, first a heater with specified parameters will be constructed and tested and the performance of other types of curved heaters is estimated based on the proposed method. Constantly increasing heater curvature increases the coefficient of performance, heat transfer, output temperature, efficiency and pressure drop. However, these parameters must be included along with the cost of construction.

References

1. Kalogirou, S.A. (2004). Solar thermal heaters and applications. Progress in Energy and Combustion Science 30: 231–295.
2. Garg, H.P., and R.S. Adhikari. (1999). Performance evaluation of a single solar air heater with N-subheaters connected in different combinations. International Journal of Energy Research 23: 403–414.
3. Duffie, J.A., and W.A. Beckman. (1991). Solar Engineering of Thermal Processes. 2nd edition. New York: John Wiley & Sons.
4. Youcef-Ali, S., N. Moummi, J.Y. Desmons, A. Abene, H. Messaoudi, and M. Le Ray. (2001). Numerical and experimental study of dryer in forced convection. International Journal of Energy Research 25: 537–53.
5. Prakash, O., and A. Kumar. (2013). Historical review and recent trends in solar drying systems. International Journal of Green Energy 10: 690–738.
6. Mahboub, C., Moummi, N., Brima, A., Moummi, A., 2015. Experimental study of new solar air heater design. Int. J. Green Energy 13, 521–529.
7. Liu, T., W. Lin, W. Gao, and C. Xia. (2007a). A comparative study of the thermal performances of cross-corrugated and v-groove solar air heaters. International Journal of Green Energy 4: 427–451.
8. Liu, T., W. Lin, W. Gao, C. Luo, M. Li, Q. Zheng, and C. Xia. (2007b). A parametric

study on the thermal performance of a solar air heater with a v-groove absorber. International Journal of Green Energy 4: 601–622.

9. Ajeet Pratap Singh, O.P. Singh. (2018). Performance enhancement of a curved solar air heater using CFD. International Journal of Solar Energy 174: 556–569.
10. Languri, E.M., H.Taherian, K. Hooman, and J. Reisel. (2011). Enhanced double-pass solar airheater with and without porous medium. International Journal of Green Energy 8: 643–654.
11. Ahmad, A., J.S. Saini, and H.K. Varma. (1996). Thermohydraulic performance of packed-bed solar air heaters. Energy Conversion and Management 37: 205–214.
12. N. Arfaoui, S. Bouadila, A. Guizani, A highly efficient solution of off-sunshine solar air heating using two packed beds of latent storage energy, Sol. Energy 155 (2017) 1243–1253, https://doi.org/10.1016/j.solener.2017.07.075.
13. Zeyu Wang, Yaohua Zhao, Chuanqi Chen, Lin Liang, Tengyue Wang. Thermal performance investigation of an integrated heater-storage solar air heater on the basis of lap joint-type flat micro-heat pipe arrays: Simultaneous charging and discharging mode[J]. Energy 2018; 181: 882-896
14. Raj AK, Srinivas M, Jayaraj S. A cost-effective method to improve the performance of solar air heaters using discrete macro-encapsulated PCM capsules for drying applications[J]. Appl Therm Eng 2019;146:910e20.
15. Abuska M, Sevik S, Kayapunar A. Experimental performance analysis of sensible heat storage in solar air heater with cherry pits/powder under the natural convection[J]. Solar Energy 2018. https://doi.org/10.1016/j.solener.2018.09.080
16. A. Ghiami, S. Ghiami, Comparative study based on energy and exergy analyses of a baffled solar air heater with latent storage heater, Appl. Therm. Eng. 133 (2018) 797–808, https://doi.org/10.1016/j.applthermaleng.2017.11.111.
17. Ajeet Pratap Singh, O.P. Singh, Curved vs. flat solar air heater: Performance evaluation under diverse environmental conditions, Renewable Energy 145 (2020) 2056–2073, https://doi.org/10.1016/j.renene.2019.07.090
18. Ajeet Pratap Singh, Akshayveer, Amit Kumar, O.P. Singh Efficient design of curved solar air heater integrated with semi-down turbulators International Journal of Thermal Sciences 152 (2020) 106304, https://doi.org/10.1016/j.ijthermalsci.2020.106304